Available online at www.sciencedirect.com
SCIENCE DIRECT®
Solid State Ionics 159 (2003) 121–134
SOLID STATE IONICS
www.elsevier.com/locate/ssi

Interfacial resistances of Ni–BCY mixed-conducting membranes for hydrogen separation

Gong Zhang[a,b,1], Stephen E. Dorris[b,*], Uthamalingam Balachandran[b], Meilin Liu[a]

[a] *School of Materials Science and Engineering, Georgia Institute of Technology, Atlanta, GA 30332, USA*
[b] *Energy Technology Division, Argonne National Laboratory, 9700 S. Cass Avenue, Building 212, Argonne, IL 60439, USA*

Received 25 March 2002; received in revised form 22 October 2002; accepted 25 October 2002

Abstract

Accurate determination of interfacial polarization resistance is essential to characterization of solid-state electrochemical systems based on thin-film electrolytes or membranes. In this study, three methods have been used to determine the interfacial resistance of a composite membrane consisting of 40 vol.% Ni and 60 vol.% $BaY_xCe_{1-x}O_3$. The interfacial resistances determined from the dependence of hydrogen permeation rate on membrane thickness were similar to those obtained from a combination of gas permeation with impedance spectroscopy (IS), implying that both approaches are applicable to the composite membrane. Results also indicate that the interfacial resistances are much greater than the bulk resistances under the conditions studied. Further improvement of the hydrogen permeation rate thus depends on reducing the interfacial polarization resistance.

PACS: 82.45.–h; 81.05.Mh
Keywords: Hydrogen separation; Mixed conductors; Interfacial polarization; Composite; Electrochemistry

1. Introduction

Mixed ionic and electronic conductors (MIECs) are widely used in solid-state electrochemical devices such as rechargeable batteries, gas sensors, fuel cells, and membrane reactors for gas separation and electrosynthesis. The overall performance of these devices depends critically on the rate of charge and mass transport through electrodes and electrolytes as well as across the interfaces. The interfacial properties, however, become more important as the thickness of the membrane is reduced. Accordingly, the interfacial polarization will eventually become the limiting factor to high performance as the membrane is made thinner.

Several techniques have been developed for characterization of interfacial polarization resistances in solid-state electrochemical devices [1–3]. Precautions have to be taken when these methods are applied to MIECs with significant electronic conductivity. In metals or composites composed of a continuous

* Corresponding author. Tel.: +1-6302525084; fax: +1-6302523604.
E-mail address: dorris@anl.gov (S.E. Dorris).
[1] Current address: UTC Fuel Cells, 195 Governors Highway, S. Windsor, CT 06074, USA.

0167-2738/02/$ - see front matter © 2002 Elsevier Science B.V. All rights reserved.
doi:10.1016/S0167-2738(02)00871-8

metallic phase, for example, the electronic transference number is so high that the open cell voltage (OCV) cannot be accurately measured, and potentiometry is no longer useful.

Early studies on a hydrogen separation membrane of similar compositions [4,5] indicate that interfacial polarization resistances dominate the overall hydrogen transport process when the samples are thin and operating temperatures are below 700 °C. Accordingly, improving hydrogen permeation necessitates accurate determination of the interfacial resistances and characterization of the interfacial processes. To date, however, no satisfactory way has been found to measure the interfacial resistance of an MIEC membrane with overwhelming electronic conduction. For a Ni–BCY composite consisting of more than 33 vol.% nickel, which exceeds the percolation threshold, the total conductivity of the composite is dominated by electronic conductivity.

In this paper, three methods have been used to determine the interfacial properties of the Ni–BCY composite membranes: (1) dependence of gas permeation on membrane thickness; (2) combination of gas permeation and impedance spectroscopy (IS); and (3) combination of potentiometry and IS. Since each method has its own advantages and limitations, the interfacial resistances determined by all three approaches will be compared.

2. Description of the three methods

It is noted that the three methods are based on the following assumptions:

(a) The ionic and electronic conductivity refers to the average conductivity across the membrane subject to a gradient in the hydrogen partial pressure.
(b) The interfacial polarization resistance remains constant with sample thickness since the same surface polishing procedures are strictly followed and all samples used in methods 1 and 2 were prepared from the same batch.
(c) The interaction between electronic and ionic carriers in the materials is neglected so that transport of the ionic defects is independent of the electronic defects.
(d) The feed and sweep gases are considered as ideal gases.
(e) Conductivity of the Ni phase does not vary much with hydrogen partial pressures, which holds true for most metals.

2.1. Method 1—dependence of gas permeation on membrane thickness

The interfacial resistance can be determined from the dependence of hydrogen permeation on membrane thickness using the following equation [6]:

$$\frac{E_N}{j_{H^+}} = \frac{\eta}{j_{H^+}} + \frac{L}{\bar{\sigma}_{amb}} \tag{1}$$

where j_{H^+} is the current density passing through the membrane due to the motion of H^+; E_N, the Nernst potential across the membrane; η, the interfacial overpotential; L, membrane thickness; and $\bar{\sigma}_{amb}$, the ambipolar conductivity averaged over the thickness. Also, in Eq. (1), $j_{H^+} = 2FN_{H_2}$, where N_{H_2} is the hydrogen permeation flux. The interfacial polarization resistance, R_p, can be determined as

$$R_p = \left(\frac{E_N}{j_{H^+}}\right)_{L\to 0} \tag{2}$$

While ambipolar conductivity can be determined as

$$\bar{\sigma}_{amb} = \left[\frac{\partial(E_N/2FN_{H_2})}{\partial L}\right]^{-1} \tag{3}$$

When (E_N/J_{H^+}) is plotted as a function of L, R_p is the intercept, and σ_{amb} is the inverse of the slope.

Note that the surface properties of all membranes with different thicknesses should be kept as constant as possible; all samples should be prepared from the same batch and the same surface processing procedures should be strictly followed. Any variation in surface properties (morphology and microstructure) from sample to sample with different thicknesses may introduce errors in determination of the interfacial resistance. Also, the accuracy of this method is limited primarily by the accuracy

with which the hydrogen permeation rates can be measured.

2.2. Method 2—Combination of gas permeation and IS

The second method combines hydrogen permeation measurements and IS [7].

$$R_e = \frac{E_N}{2I_{H^+}} - \sqrt{\left(\frac{E_N}{2I_{H^+}}\right)^2 - R_t\left(\frac{E_N}{2I_{H^+}}\right)} \quad (4)$$

$$R_{H^+} = \frac{R_b R_e}{R_b + R_e} \quad (5)$$

$$R_p = \frac{E_N}{I_{H^+}} - R_e - R_{H^+} \quad (6)$$

where R_b is the resistance of the bulk electrolyte, and I_{H^+} is the proton current. The electronic resistance of the sample can be calculated from the total resistivity of a bar sample since the electronic conductivities are much greater than the ionic conductivities ($\sigma_e \gg \sigma_i$), and thus $\sigma_T \approx \sigma_e$. A bar sample with a large aspect ratio is used to increase the accuracy of the impedance measurement. Impedance spectra were collected in a uniform atmosphere (4% H_2/nitrogen) for this study. In each spectrum, only a point was observed without a typical impedance loop, confirming that the electronic resistance is much smaller than the ionic resistance, and the total resistance is approximately equal to the electronic resistance. The ionic resistance can be calculated from the ionic conductivity and the dimensions of the membrane. Finally, the interfacial polarization resistance can be calculated in Eq. (6). The accuracy of method 2 depends on the accuracy of the permeation measurements and the validity of the assumption that the electronic conductivity of the Ni phase does not vary much with hydrogen partial pressures, which holds true for most metals.

2.3. Method 3—Combination of potentiometry and IS

The combination of OCV measurements and impedance spectroscopy can be used to determine the interfacial polarization resistance, as follows [8]:

$$R_p = \frac{R_t E_N}{V_{OC}} - R_i = \frac{R_t - R_b}{\frac{V_{OC}}{E_N}\left[1 - \frac{R_b}{R_t}\left(1 - \frac{V_{OC}}{E_N}\right)\right]} \quad (7)$$

where R_t is the total resistance, and R_i the bulk resistance for the ionic species. Both R_b and R_t can be readily determined from an impedance spectrum, and V_{OC} from an OCV measurement. Since the composite membrane cannot be used as an electrolyte in an OCV measurement due to its predominant electronic conductivity, an electrochemical cell, with a configuration of MIEC (Ni–BCY)|proton conductor (pure BCY)|MIEC (Ni–BCY), was built to measure the OCV. The same BCY powders, used in the composite membrane, were pressed into pellets and then sintered. The sintered pellets were polished to 1.2 mm, and the Ni–BCY was screen-printed on both sides of the pure BCY electrolyte and sintered at 1420 °C for 1 h in 4% H_2. Platinum mesh was used as the current collectors.

Method 3 attempts to measure the interfacial resistance indirectly. The simulated interface in the electrochemical cell includes the Ni–BCY composite, BCY electrolyte, and gas phase. The simulated interface differs from that of the actual separation membrane, which constitutes only the Ni–BCY composite and gas phase. Due to the difference in the composition and microstructure between these two interfaces, the measured interfacial resistance of the electrochemical cell could be quite different from that of the actual interface. As a result, the accuracy of this method largely depends on the closeness of the simulated interface to the hydrogen separation membrane.

3. Experimental

3.1. Sample preparation

The Ni–BCY composite membranes were prepared as described elsewhere [9]. Before any surface modifications, both sides of each sintered pellet were polished to the desired thickness using #600 grit

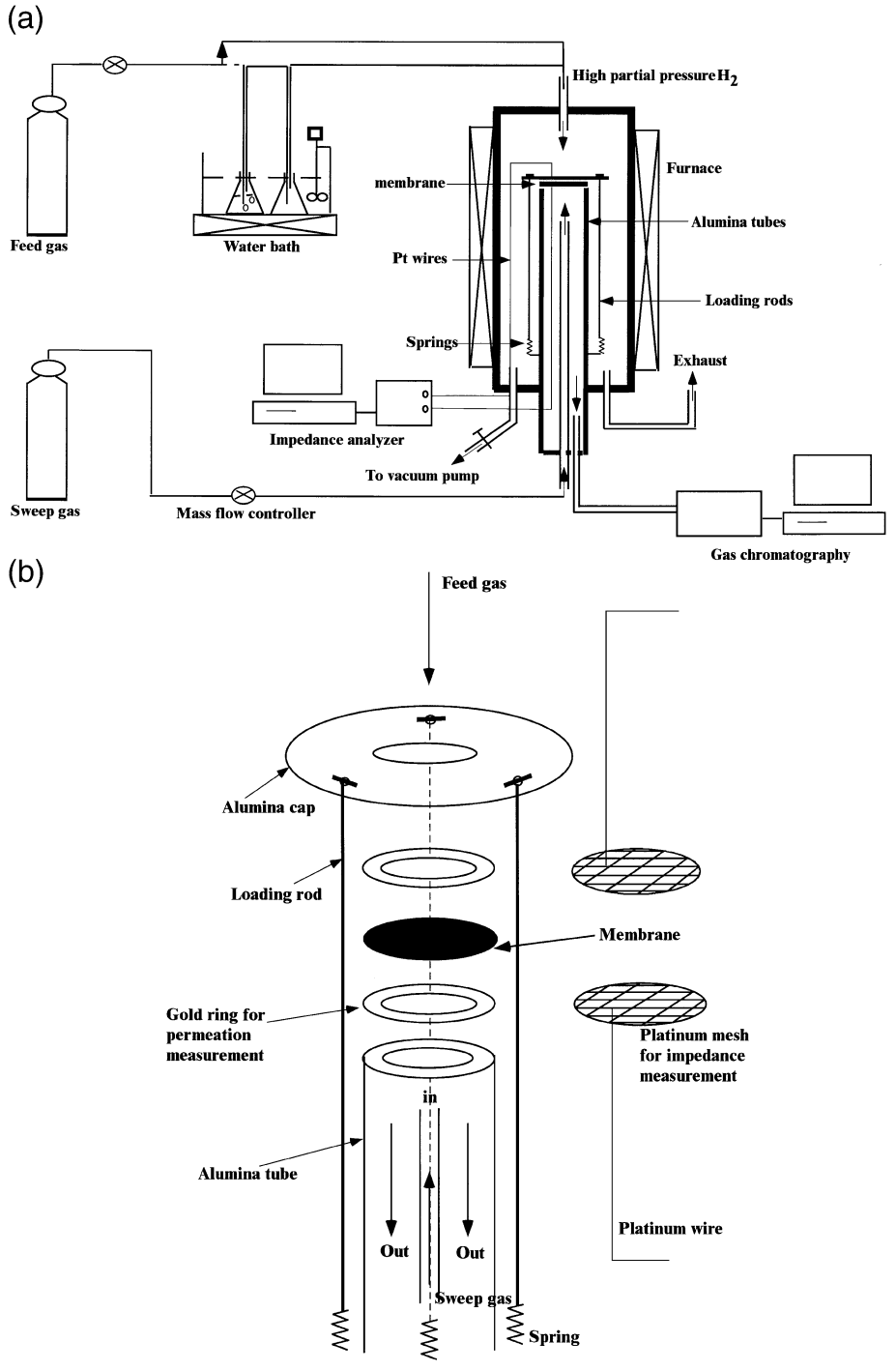

Fig. 1. (a) Schematic set up for electrochemical characterization of gas permeation membranes and (b) zoom-in view of the membrane sealing and loading.

sandpaper. To ensure the consistency of the surface conditions in the permeation measurement, all samples were prepared from the same batch, and the same surface processing procedures were strictly followed. Thicknesses of the samples used in method 1 were 0.019, 0.041, and 0.071 cm. The pure BCY electrolytes used in method 3 were prepared in a similar way, starting with the BCY powders and sintering at 1420 °C in 4% H_2 for 6 h.

3.2. Electrochemical characterization

Shown in Fig. 1 is the self-built test set up for electrochemical characterization of gas permeation membranes. The samples were sealed on an alumina tube using gold rings. The feed gas was composed of hydrogen of different partial pressures (4%, 30%, 99%) balanced with helium, and the sweep gas contained 100 ppm hydrogen balanced with nitrogen to prevent the oxidation of nickel phase in the composite. The flow rates on both sides were maintained at 100 cc min^{-1} with the sweep gas flow rate controlled by an MKS 1179A mass flow controller. The hydrogen partial pressure in the sweep gas was analyzed by a gas chromatograph (Hewlett-Packard 6890). The composition, microstructure, and surface morphology of the membrane were examined using a scanning electron microscope (SEM, JEOL JSM-5400) equipped with an energy dispersion X-ray (EDX) analyzer. A Solartron SI 1260 was used for impedance measurements in the frequency range from 10^7 to 0.01 Hz.

3.3. Building an electrochemical cell in method 3

An electrochemical cell was built with pure BCY electrolytes for simultaneous OCV and impedance measurements. Both surfaces of BCY electrolyte pellets were ground with 600-grit sandpaper to 1.2-mm thickness. Ni–BCY composite powders were

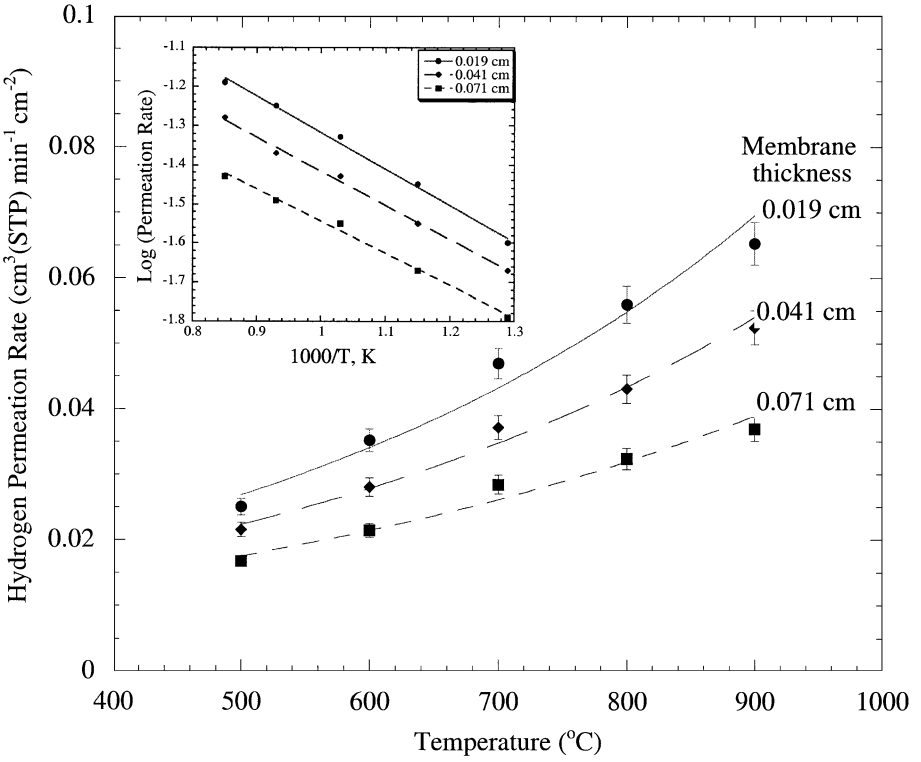

Fig. 2. Hydrogen permeation rate through the Ni–BCY composite membranes of various thicknesses as a function of temperatures.

mixed with the ethylene glycol and isopropyl alcohol (IPA) at a volume ratio 1:10:1, then screen printed onto the surfaces of the BCY pellets to form electrodes. After drying, the electrodes were fired at 1420 °C for 1 h in 4% H_2. Platinum meshes, used as current collectors, were attached with Pt leads and loaded as shown in Fig. 1b for electrochemical characterizations.

4. Results

4.1. Method 1—dependence of gas permeation on membrane thickness

Shown in Fig. 2 are the hydrogen permeation rates through Ni–BCY membranes with different thickness and temperatures of 500 to 900 °C (4% H_2 as feed gas). The permeation fluxes increased with temperature for all samples. The temperature dependence of permeation, however, is low, suggesting the low activation energy of the proton transport in the bulk. Eqs. (1)–(3) can be used to determine the ambipolar conductivity and interfacial polarization resistance from the dependence of the hydrogen permeation rate on membrane thickness. Based on the permeation rate in Figs. 2, 3 plots $E_N/(2FN)$ against sample thickness L. According to the Eq. (2), the overall interfacial resistance associated with the hydrogen separation is the interception of the line extrapolated to zero thickness ($L \rightarrow 0$), while the slope of Fig. 3 gives the ambipolar conductivity of the membranes. The interfacial resistances decreased with temperatures from 63.2 Ω cm^2 at 500 °C to 35.4 Ω cm^2 at 900 °C. The ambipolar conductivity of the membrane increased with temperature, ranging from 0.0014 S cm^{-1} at 500 °C to 0.0019 S cm^{-1} at 900 °C.

4.2. Method 2—combination of gas permeation measurement and IS

The electronic conductivity of Ni–BCY has to be measured in order to determine the interfacial

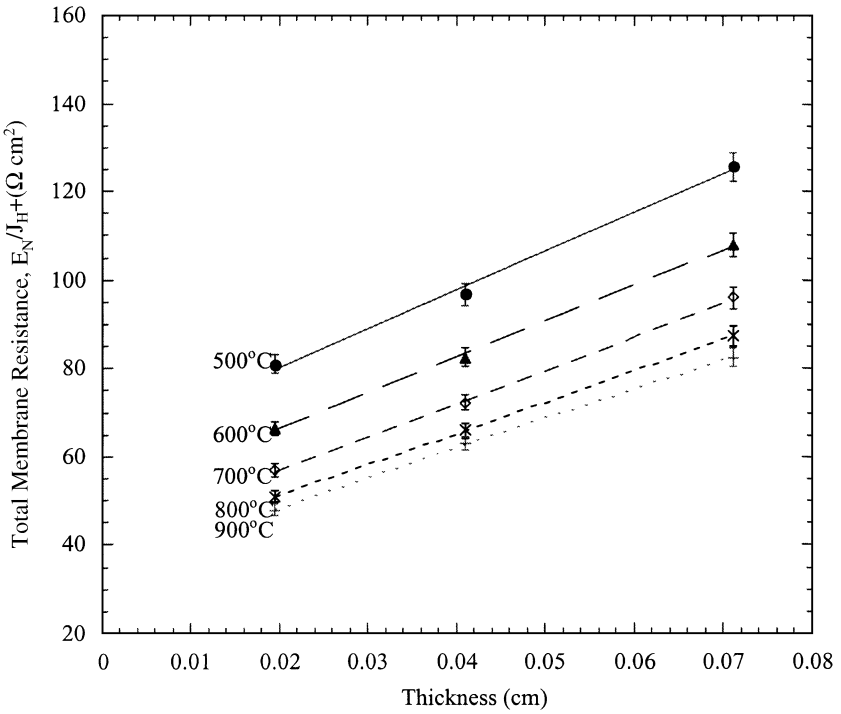

Fig. 3. Thickness dependence of total membrane resistance, E_N/J_{H^+}, under the same conditions for hydrogen permeation as in Fig. 2.

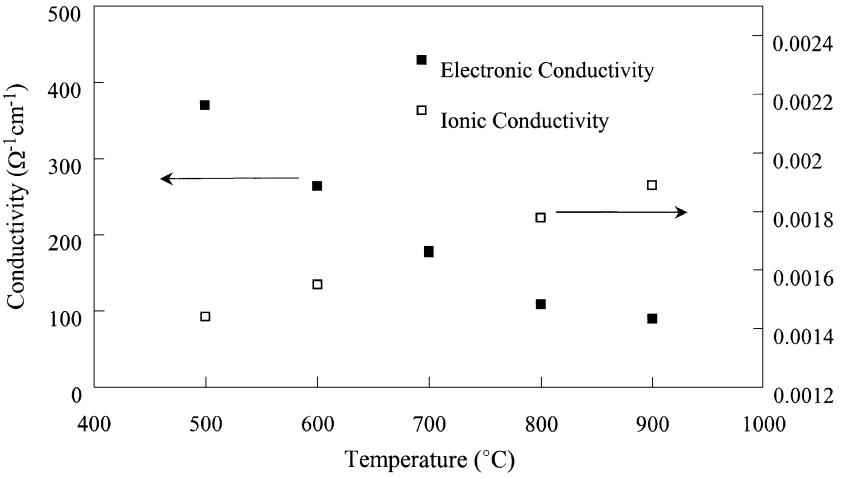

Fig. 4. Ionic and electronic conductivity of Ni–BCY composite sample.

resistance. As shown in Fig. 4, the electronic conductivity of the composite, calculated from a bar sample with a high aspect ratio, decreased from 370 $\Omega^{-1}\text{cm}^{-1}$ at 500 °C to 89 $\Omega^{-1}\text{cm}^{-1}$ at 900 °C. Compared with the conductivity data of pure nickel reported in the literature, the conductivity of the composite bar is about two orders of magnitude smaller. Wu and Liu [10] modeled the ambipolar transport properties of metal–ceramic composites. In this model, the effective electronic conductivity of a composite can be calculated from the following equation:

$$\sigma_{\text{m}}^{\text{e}} = \frac{E_1^{\text{e}} + \sqrt{(E_1^{\text{e}})^2 + E_2^{\text{e}}}}{4} \tag{8}$$

where

$$E_1^{\text{e}} = 3(p_1\sigma_1^{\text{e}} + p_2\sigma_2^{\text{e}}) - (\sigma_1^{\text{e}} + \sigma_2^{\text{e}}),$$

$$E_2^{\text{e}} = 8\sigma_1^{\text{e}}\sigma_2^{\text{e}},$$

p_1 and p_2 are the volume fraction of the electronic and ionic conducting phases, respectively, and σ_1^{e} and σ_2^{e} are the electronic conductivity of the respective phases. From Eq. (8), the calculated conductivity of the Ni–BCY composite is approximately 0.1 σ_1^{e}, which is an order of magnitude greater than the measured conductivity of the Ni–BCY composite. The difference between them is due to the different processing procedures used to prepare the composite and microstructures thus obtained. The conductivity of cermet also depends on a number of other factors, such as nickel content, pore fraction, and interactions between the charge carriers, etc. The specific reason for the difference between these two systems is not clear.

The ionic conductivity as shown in Fig. 4 was derived from Eq. (5), and the conductance was calculated based on a sample area of 1.27 cm^2 and thickness of 0.019 cm. Finally, the interfacial resistance was calculated from Eq. (6).

4.3. Method 3—combination of potentiometry and IS

Since the open cell voltage across a Ni–BCY composite membrane cannot be measured under the permeation conditions, an electrochemical cell consisting of Ni/BCY/Ni with similar interfaces, simulating that in the composite membrane with gas phases, was built and tested under the same conditions for hydrogen permeation measurements, i.e. 4% H_2 in the feed gas vs. 100 ppm in the sweep gas. Fig. 5 shows the impedance spectra of the cell measured at 500 to 900 °C. The impedance shows severely depressed semicircles. Both the bulk and total resistances, as determined from the intercepts of the impedance spectra with the *X*-axis, decrease with temperature. The impedance between the two intercepts in the spectra can be used to determine the interfacial polarization resistance if the electrolyte is

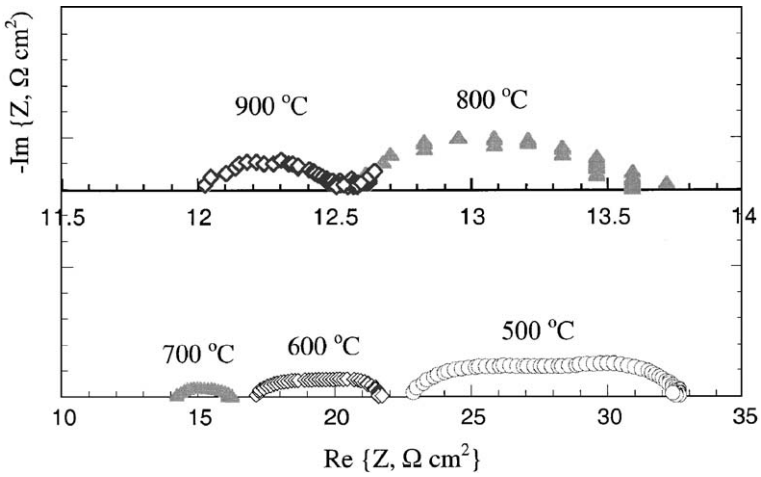

Fig. 5. Typical impedance spectra of the electrochemical cell at different temperatures. Configuration of the cell: 4% H_2, Ni–BCY|BCY|Ni–BCY, 100 ppm H_2.

a purely ionic conductor. For MIECs, like pure BCY with a substantial electronic conductivity present at high temperatures, the determination of interfacial resistance has to be combined with Nernst potential and OCV measurements of the same cell. Shown in Fig. 6 are the Nernst potentials and OCVs across the electrochemical cell. The OCV/E_N ratio becomes smaller with temperature because the electronic conductivity increases faster than the ionic conductivity with temperature. The data shown in Figs. 5 and 6

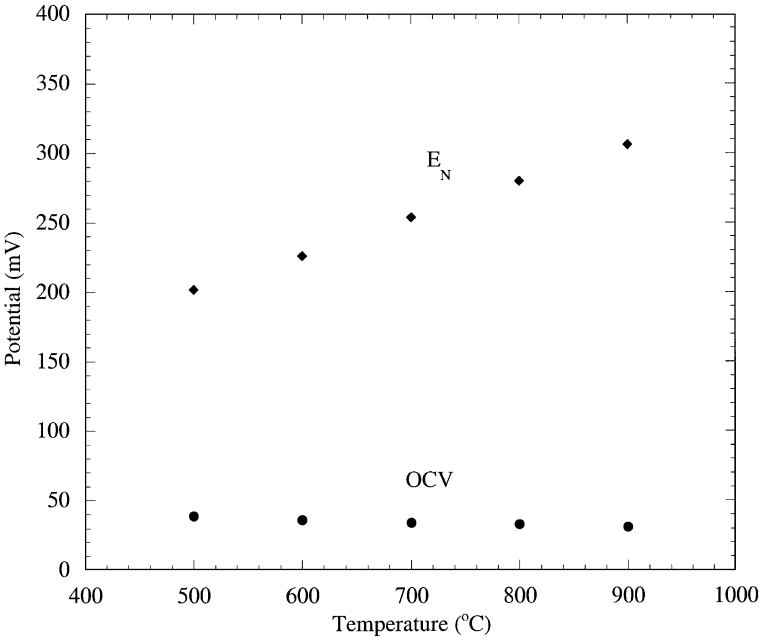

Fig. 6. Nernst potential and open cell voltage (OCV) across the electrochemical cell under the same conditions as used for hydrogen permeation measurements.

allow determination of the interfacial resistance using Eq. (7).

5. Discussion

5.1. Comparison of the three methods

Shown in Fig. 7 are the interfacial resistances determined by the three methods. With methods 1 and 2, the interfacial resistances changed from 62.9–53.3 Ω cm^2 at 500 °C to 35.2–28.8 Ω cm^2 at 900 °C. In contrast, with method 3, the interfacial resistances decreased dramatically with temperature, from 115 Ω cm^2 at 500 °C to 33 Ω cm^2 at 900 °C. Clearly, the interfacial resistances as determined by the first two methods differ markedly from those determined by the third, especially at low temperatures, even though all of them show a similar trend of decreasing resistance with temperature. These differences are attributed to the differences in the nature of the interfaces studied. Fig. 8 shows the surface view of the composite membrane for methods 1 and 2, and surface and cross-sectional views of

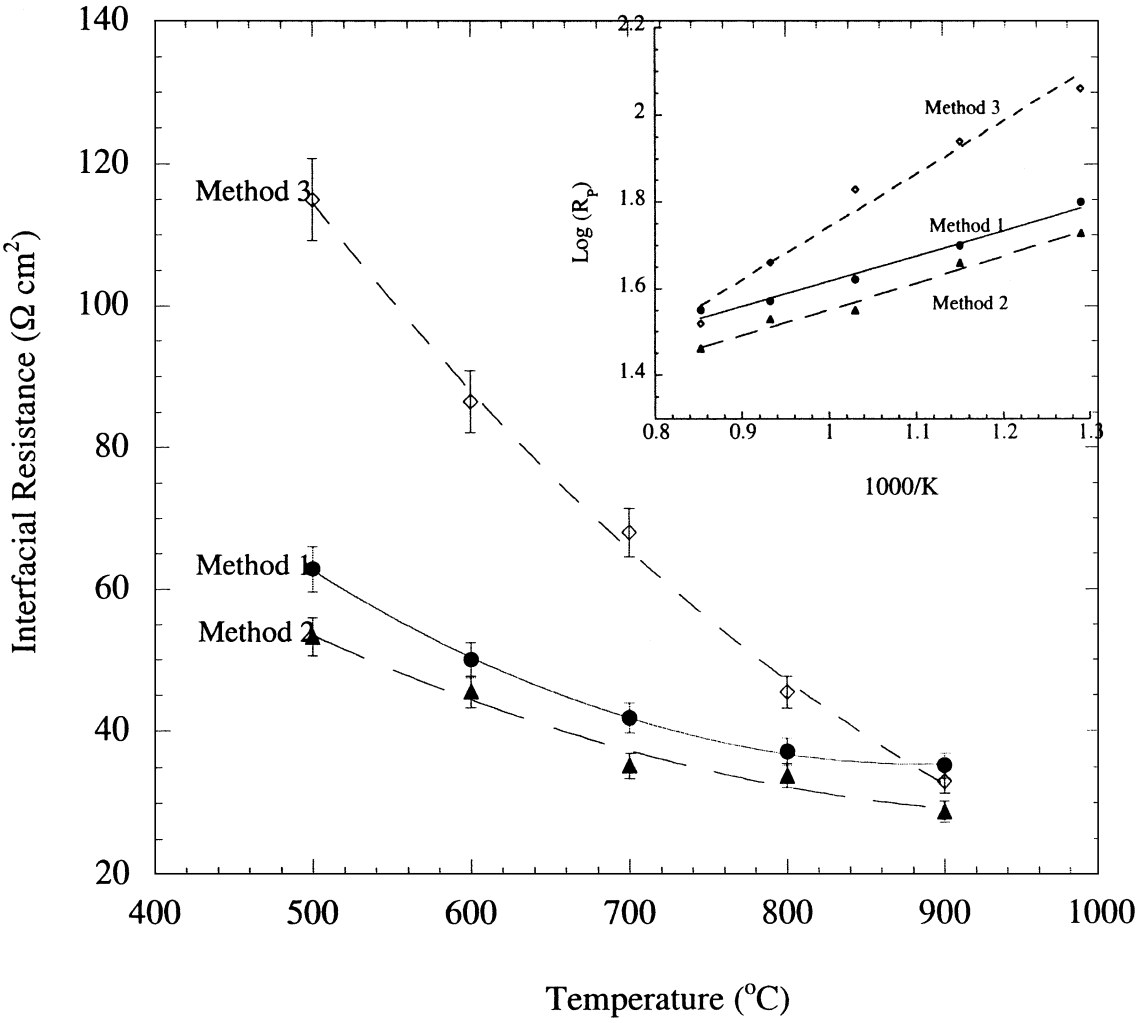

Fig. 7. Comparison of interfacial resistances measured by three different methods.

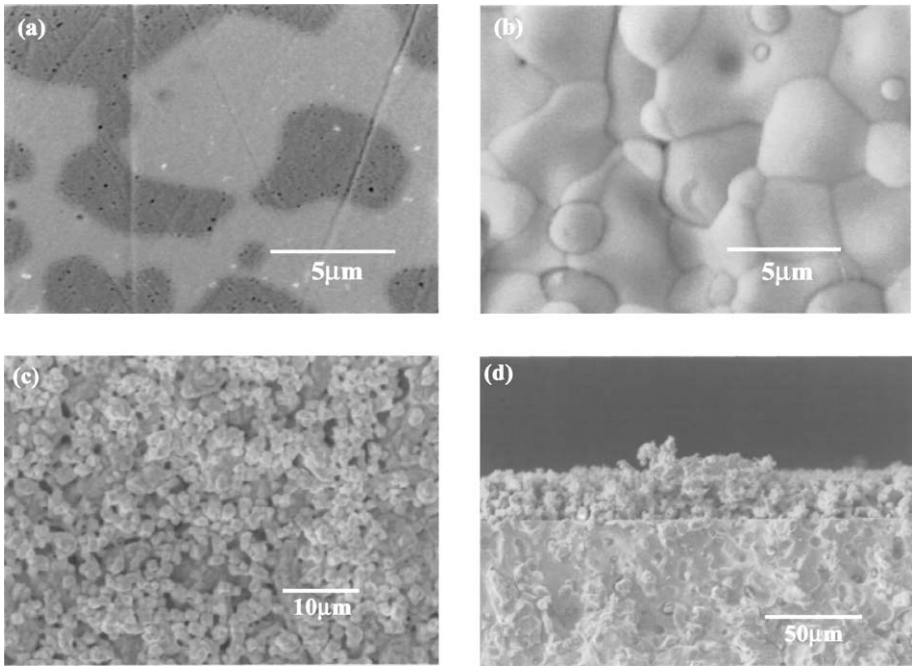

Fig. 8. SEM pictures of surface and cross-sectional views of the composite membrane and electrodes on the cells for the third method: Surface views of (a) the composite membrane, (b) BCY electrolyte of the cell, (c) electrodes on the cell, and (d) cross-sectional view of the cell.

the cells for method 3. Clearly, the interfaces of the composite membrane are composed of Ni–BCY–hydrogen interface whereas another pure BCY electrolyte/electrode interface is added in the third method, which may introduce a severely polarizable interface. The electrolyte of the cell shows distinctively defined grain boundaries; the membrane surface, however, only shows boundaries between nickel and BCY dense phases. The electrode on the cell has a highly porous microstructure, quite different from the surfaces of dense composite membranes. These differences in microstructure between the surface of the composite membrane and the interfaces of the cell lead to the large variations in interfacial polarization resistances measured by these methods.

5.2. Domination of interfacial resistance over bulk resistance

Shown in Fig. 9 is the comparison of interfacial resistances with bulk ionic resistances of Ni–BCY composite membranes of different thicknesses as a function of temperature. Since methods 1 and 2 give close results, method 1 was chosen to represent the interfacial resistance. Between 500 and 900 °C, the interfacial and bulk resistances decrease with temperature; the interfacial resistance R_p dropped from 62.7 Ω cm^2 at 500 °C to 35.2 Ω cm^2 at 900 °C, whereas the bulk resistance dropped from 12.5 Ω cm^2 at 500 °C to 9.5 Ω cm^2 at 900 °C for a membrane of 0.019-cm thickness. The ratio of the interfacial to the bulk resistance is about 5 at 500 °C and 3.7 at 900 °C; these values imply that the interfacial resistances dominate the total resistance of the membrane to hydrogen permeation at the temperature range studied. The ionic resistances increase proportionally with the thickness of the membranes, whereas the interfacial resistances remain the same. For the 0.041-cm-thick sample, the interfacial resistances still dominate at all temperatures, but the ratio of the interfacial resistance to the bulk resistance decreases to 2.3 at 500 °C and 1.7 at 900 °C. As the thickness increases further to 0.071 cm, the bulk resistances are compa-

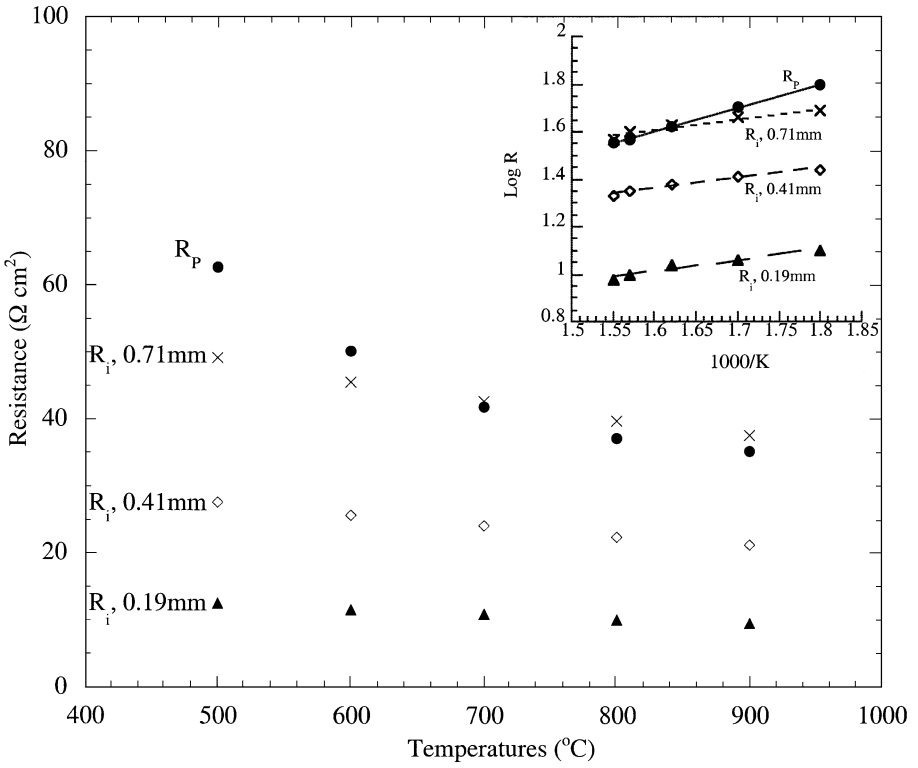

Fig. 9. Comparison of interfacial and ionic resistance of Ni–BCY composite membranes measured at different temperatures with 4% H_2 as the feed gas and 100 ppm H_2 as the sweep gas.

rable to the interfacial resistance at temperatures higher than 700 °C. While the bulk resistance can be reduced by making the membrane thinner; the interfacial resistance determines the hydrogen permeation rate, especially when the membrane is thin. Reducing the interfacial resistance, therefore, is the next challenge to further improve the hydrogen permeation rate.

The interfacial and bulk resistances of the Ni–BCY membranes depend strongly on the partial pressure of hydrogen. Shown in Fig. 10 are the interfacial and ionic resistances of Ni–BCY composite membranes of different thicknesses for a hydrogen partial pressure in the feed gas of 30%. Compared with the data in Fig. 9, all resistances decreased with the increased partial pressure of hydrogen. The partial pressure of hydrogen may influence the interfacial resistance in two ways. First, the H_2 partial pressure may directly influence the kinetics of the hydrogen oxidation occurring at the interfaces. Further, a change in H_2 partial pressure may change the defect chemistry at the membrane surface and influence the surface catalytic properties. Second, higher hydrogen partial pressure also increases the driving force for proton transportation, resulting in a non linear increase in hydrogen permeation since the charge transfer resistance increases exponentially with the driving force according to the B-V equation.

The hydrogen partial pressure is also a critical factor in determining the ratio of interfacial to ionic resistance. Fig. 11 shows the interfacial and ionic resistance of the Ni–BCY composite membranes of different thicknesses measured with 99% H_2 as the feed gas. Compared with the results at 4% H_2 (Fig. 9), the interfacial resistance decreases from 62.7 to 34.9 Ω cm^2 at 500 °C and from 35.2 to 24.2 Ω cm^2 at 900 °C. The decrease is more dramatic in the low temperature range (500–600 °C) than in the high temperature range (800–900 °C), indicating that the interfacial resistance is more severe at low temper-

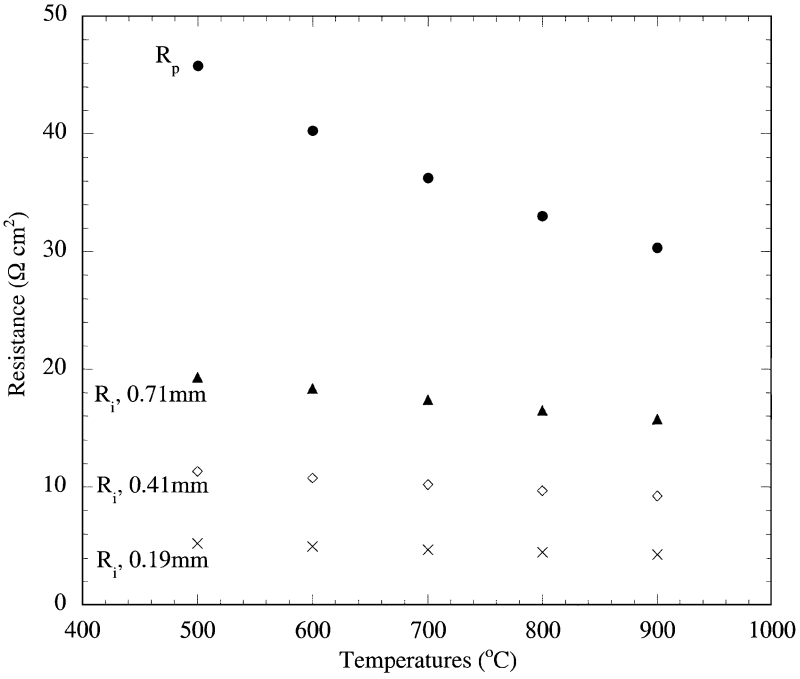

Fig. 10. Comparison of interfacial resistance and ionic resistance of Ni–BCY composite membranes measured at different temperatures with 30% H_2 as the feed gas and 100 ppm H_2 as the sweep gas.

atures. The ionic resistance in the bulk also shows a decrease with H_2 partial pressures, for example, from 12.47 Ω cm^2 at 4% H_2 to 4.33 Ω cm^2 at 99.9% H_2 for the membrane of 0.019-cm thickness. Compared with the change of interfacial resistance, the ionic resistance decreases more in terms of percentage change. As a result, the interfacial resistance plays a more important role when hydrogen partial pressure is high. With 4% hydrogen as the feed gas for a sample of 0.071-cm thickness, the interfacial and ionic resistances each contribute approximately one-half of the overall resistance at temperatures higher than 700 °C. With 99.9% hydrogen as the feed gas, however, the ratio of interfacial to ionic resistance is about 2 at the temperatures examined for membranes of the same thickness. With hydrogen partial pressure increasing, both interfacial and ionic resistance decrease, but at different rates. Ionic resistance drops much faster than interfacial resistance so that interfacial resistance dominates the hydrogen separation process when the hydrogen partial pressure in the feed gas is 30% or higher, regardless of the membrane thickness. The increase in bulk conductivity with hydrogen partial pressure can be explained by the change in the charge carrier concentration in the bulk materials. With hydrogen partial pressure increasing, as explained in the last section, the interfacial resistance decreases, and thus, more protons are expected to incorporate into the bulk materials. Protons, as the main ionic charge carrier species for cerate-based materials in a reducing atmosphere, increase with hydrogen partial pressure, and thus, so does the conductivity of the bulk materials.

Regardless of the hydrogen partial pressure in the feed gas, the interfacial resistance dominates the overall resistance of hydrogen separation for samples less than 0.071 cm, more so when the membranes are thinner. For a membrane with 0.019-cm thickness, the ratio of interfacial to ionic resistance increases to 8.5 at 500 °C with 99% hydrogen as the feed gas. Besides the membrane thickness and temperature, hydrogen partial pressure is a critical factor in determining the ratio of interfacial to ionic resistance. As shown above, the surface polarization resistance is the dominant resistance to the hydrogen transport process under the electrochemical conditions studied.

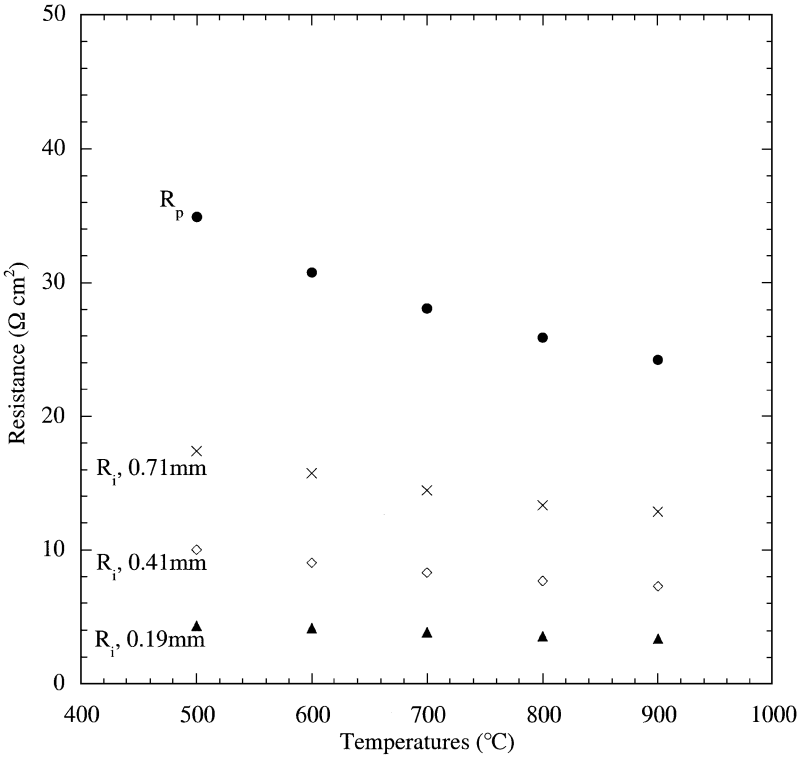

Fig. 11. Comparison of interfacial resistance and ionic resistance of Ni–BCY composite membranes at different temperatures with 99.9% H_2 as the feed gas and 100 ppm H_2 as the sweep gas.

To further improve hydrogen permeation, it is essential to lower the surface polarization resistance.

6. Conclusions

Three methods have been used to measure the interfacial resistances of the Ni–BCY composite membrane, an MIEC with predominantly electronic conductivity. Results show that the first two methods (hydrogen permeation vs. membrane thickness and a combination of hydrogen permeation with IS) are applicable to this composite membrane, whereas the third method (combination of potentiometry and IS) is not. The differences in interfacial resistances are expectedly due to the differences in the nature of the interface studied. Temperature, membrane thickness, and hydrogen partial pressure were found to be the three major factors influencing the ratio of interfacial to bulk resistance. Interfacial resistances dominate at temperatures below 700 °C or when the membrane is thinner than 0.071 cm. As hydrogen partial pressure increases from 4% to 99%, the ionic resistances decrease much faster than the interfacial resistances. As a result, interfacial resistance dominates the separation process when the feed gas contains a hydrogen partial pressure higher than 30% for membranes with all thicknesses.

Lists of symbols

E_N	Nernst potential (V)
F	Faraday's constant, 9.6485 (C equiv^{-1})
I_{H^+}	proton current (A)
j_{H^+}	proton current density (A cm^{-2})
L	sample thickness (cm)
p_1 and p_2	volume fraction of the electronic and ionic conducting phases
R_b	resistance of bulk electrolyte (Ω)
R_e, R_i	bulk resistance to the motion of electronic and ionic species, respectively (Ω)

R_t total resistance of an electrochemical cell shown in the impedance spectra (Ω)
$\bar{\sigma}_{amb}$ ambipolar conductivity (S cm^{-1})
σ^e electronic conductivity
T absolute temperature (K)
η interfacial overpotential, respectively (V)

Abbreviations

BCY $Ba_{0.8}Y_{0.2}CeO_3$
Ni–BCY 40 vol.% nickel–60 vol.% $Ba_{0.8}Y_{0.2}CeO_3$
IS Impedance spectra
MIEC mixed ionic-electronic conductor
OCV open cell voltage

Acknowledgements

This work is supported by the U.S. Department of Energy, National Energy Technology Laboratory, under contract W-31-109-Eng-38.

References

[1] H. Hu, M. Liu, J. Electrochem. Soc. 144 (10) (1997) 3561–3567.
[2] K. Yasumoto, N. Mori, J. Mizusaki, H. Tagawa, M. Dokiya, J. Electrochem. Soc. 148 (1) (2001) A105–A111.
[3] S.P. Jiang, J.G. Love, Solid State Ionics 138 (2001) 183–190.
[4] J. Guan, S.E. Dorris, U. Balachandran, M. Liu, Solid State Ionics 100 (1997) 45–52.
[5] J. Guan, S.E. Dorris, U. Balachandran, M. Liu, Solid State Ionics 110 (1998) 3–4, 303–310.
[6] M. Liu, A. Joshi, in: T.A. Ramanarayanan, H.L. Tuller (Eds.), Proc. 1st Int. Symp. on Ionic and Mixed conducting Ceramics, Electrochemical Society, Pennington, NJ, 1991, pp. 231–245, 91–12.
[7] M. Liu, B. Rauch, unpublished work.
[8] M. Liu, H. Hu, J. Electrochem. Soc. 143 (6) (1996) L109.
[9] G. Zhang, S.E. Dorris, U. Balachandran, M. Liu, unpublished work.
[10] Z. Wu, M. Liu, Solid State Ionics 93 (1–2) (1996, Dec.) 65–84.